Title

Osteophytes and fracture calluses share developmental milestones and are diminished by unloading

Journal

Journal of Orthopaedic Research®, 36(2)

ISSN

0736-0266

Authors

Hsia, Allison W
Emami, Armaun J
Tarke, Franklin D
et al.

Publication Date

2018-02-01

DOI

10.1002/jor.23779

Peer reviewed

HHS Public Access

Author manuscript

J Orthop Res. Author manuscript; available in PMC 2019 February 01.

Published in final edited form as:

J Orthop Res. 2018 February ; 36(2): 699–710. doi:10.1002/jor.23779.

Osteophytes and fracture calluses share developmental milestones and are diminished by unloading

Allison W. Hsia, M.Eng.[(1)], **Armaun J. Emami, M.S.**[(1)], **Franklin D. Tarke**[(2)], **Hailey C. Cunningham, B.S.**[(1)], **Priscilla M. Tjandra, B.S.**[(1)], **Alice Wong, Ph.D.**[(3)], **Blaine A. Christiansen, Ph.D.**[(1),(2),*], and **Nicole M. Collette, Ph.D.**[(4),*]

[(1)]Biomedical Engineering Graduate Group, University of California Davis, Davis, CA

[(2)]Department of Orthopaedic Surgery, University of California Davis Medical Center, Sacramento, CA

[(3)]Department of Anatomy, Physiology, and Cell Biology, School of Veterinary Medicine, University of California, Davis, CA

[(4)]Biosciences and Biotechnology Division, Lawrence Livermore National Laboratory, Livermore, CA

Abstract

Osteophytes are a typical radiographic finding during osteoarthritis (OA), but the mechanisms leading to their formation are not well known. Comparatively, fracture calluses have been studied extensively, therefore drawing comparisons between osteophytes and fracture calluses may lead to a deeper understanding of osteophyte formation. In this study we compared the time courses of osteophyte and fracture callus formation, and investigated mechanisms contributing to development of these structure. Additionally, we investigated the effect of mechanical unloading on the formation of both fracture calluses and osteophytes. Mice underwent either transverse femoral fracture or non-invasive anterior cruciate ligament rupture. Fracture callus and osteophyte size and ossification were evaluated after 3, 5, 7, 14, 21, or 28 days. Additional mice were subjected to hindlimb unloading after injury for 3, 7, or 14 days. Protease activity and gene expression profiles after injury were evaluated after 3 or 7 days of normal ambulation or hindlimb unloading using *in vivo* fluorescence reflectance imaging (FRI) and quantitative PCR. We found that fracture callus and osteophyte growth achieved similar developmental milestones, but fracture calluses formed and ossified at earlier time points. Hindlimb unloading ultimately led to a 3-fold decrease in chondro/osteophyte area, and a 2-fold decrease in fracture callus area. Unloading was also associated with decreased inflammation and protease activity in injured limbs detected with

Corresponding authors: Blaine A. Christiansen, Ph.D., University of California Davis Medical Center, 4635 2nd Avenue, Suite 2000, Sacramento, CA 95817, bchristiansen@ucdavis.edu, Tel: (916) 734-3974, Fax: (916) 734-5750. Nicole M. Collette, Ph.D., Lawrence Livermore National Laboratory, 7000 East Avenue, L-452, Livermore, CA 94550, collette2@llnl.gov, Tel: (925) 423-2353, Fax: (925) 422-2099.

Author contributions:

AWH performed ACL rupture injuries, collected osteophyte and fracture callus volume, area, and ossification area, was primarily responsible for data analysis and manuscript writing, and contributed to study design. AJE performed fracture surgeries. FDT assisted with fracture surgeries, ACL rupture injuries, and sample collection. HCC, AW, and PMT assisted with sample and data collection. BAC coordinated all analyses, assisted with study design, and contributed to manuscript writing. NMC performed histology and contributed to both study design and manuscript writing.

FRI, particularly following ACL rupture. qPCR analysis revealed disparate cellular responses in fractured femurs and injured joints, suggesting that fracture calluses and osteophytes may form via different inflammatory, anabolic, and catabolic pathways.

Graphical Abstract

This study compared the time courses and underlying mechanisms contributing to fracture callus and osteophyte formation in mice after femoral fracture or ACL rupture, respectively. Formation of these structures shared developmental milestones, but progressed on slightly different timelines. Both structures depended on mechanical stimuli; hindlimb unloading resulted in reduced callus and osteophyte size, inflammation, and protease activity. However, the cellular response of these structures differed at early time points, suggesting disparate formation pathways.

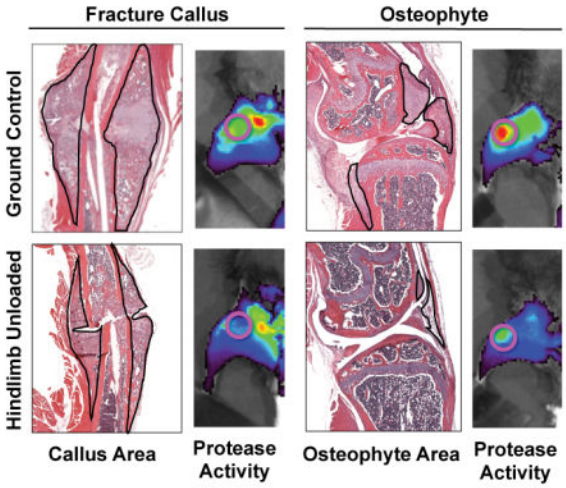

Keywords

post-traumatic osteoarthritis; osteophytes; fracture healing; hindlimb unloading

Introduction

Osteoarthritis (OA) is a leading cause of disability worldwide, and affects approximately 27 million people in the United States [1]. OA patients suffer debilitating pain and decreased joint range of motion (ROM) associated with articular cartilage degeneration, subchondral bone sclerosis, and osteophyte formation [2]. Osteophytes are bony outgrowths that form at joint margins and are considered a typical radiographic finding of OA that may contribute to decreased joint range of motion and pain. Osteophytes begin as cartilaginous growths, or chondrophytes, that subsequently undergo intramembranous and endochondral ossification. Mature osteophytes are mineralized and fully integrated with native bone, covered by articular cartilage which extends from the articular surface [3, 4]. Osteophyte formation is strongly affected by both mechanical and biological factors. Previous animal studies have shown that osteophyte growth increases with exercise and is inhibited by immobilization [5–8], restoring natural joint kinematics after anterior cruciate ligament (ACL) transection decreases osteophyte growth [9], and modulating expression of transforming growth factor-

beta 1 (TGF-β1) in the murine joint leads to changes in osteophyte development [10, 11]. These characteristics of osteophytes have led previous studies to hypothesize that osteophytes are analogous to fracture calluses, but no formal comparison has been performed [12].

The formation of fracture calluses and osteophytes are generally similar, and recapitulate the differentiation pattern in the growth plate during development [13, 14]. Both begin as cartilaginous soft tissue that gradually ossifies to become bone [3, 15], both are highly modulated by the TGF-β superfamily [10, 11, 16], and both are thought to act as mechanical stabilizers [17–21]. We previously showed that chondro/osteophyte formation after injury correlates with increasing joint stability after ACL rupture in mice, with a full return to control levels after 8 weeks [20]. These results followed a similar time course to bone restabilization by callus formation, during which full restabilization has been found to occur after 8 weeks in rats and at least 28 days in mice [22, 23]. Furthermore, fracture callus formation has been shown to depend on normal loading during ambulation, with unloaded fractures leading to smaller calluses [21, 24]. Mechanisms of fracture healing have been much more thoroughly characterized than osteophyte formation, with a plethora of studies investigating mechanical and biological factors in callus formation [21]. Therefore, identifying similarities and differences between osteophyte development and fracture healing may lead to revelations regarding mechanisms of osteophyte formation and their clinical treatment.

In this study, we compared osteophyte formation following non-invasive ACL rupture and fracture callus formation following femur fracture in mice. Mineralized osteophyte and fracture callus volume and tissue mineral density (TMD) were evaluated using micro-computed tomography, and histology was used to visualize chondrophyte and soft callus area and composition. *In vivo* fluorescence reflectance imaging (FRI) was used to visualize protease activity and inflammation, and quantitative polymerase chain reaction (qPCR) examined gene expression after injury. The role of ambulatory loading in osteophyte and fracture callus formation was also evaluated through hindlimb unloading of mice. We hypothesized that (1) chondro/osteophytes would form and ossify on a similar time scale to fracture calluses, (2) that osteophytes, like fracture calluses, would require mechanical stimuli to form, (3) that osteophytes and fracture calluses would form via activation of similar inflammatory, anabolic, and catabolic pathways, and (4) that hindlimb unloading would lead to reduced activation of inflammatory and anabolic pathways while promoting catabolic gene expression.

Methods

Animals

111 skeletally mature (12-weeks-old at injury; [25]) female C57BL/6 mice were obtained from Envigo (Indianapolis, IN) and were acclimated for one week period before injury. Mice were subjected to either non-invasive ACL rupture or transverse femoral fracture prior to euthanasia at 3, 5, 7, 14, 21, or 28 days post-injury (n=5–6/injury/time point) via CO_2 inhalation. Additional mice for day 3, 7, and 14 time points were injured via ACL rupture or femur fracture and subject to hindlimb unloading (HLU) via tail suspension to examine the

effect of mechanical unloading on osteophyte and fracture callus formation (n=5–6/injury/time point). Six mice were euthanized before the end of the study due to complications associated with femur fracture or HLU. Mice were maintained and used in accordance with National Institutes of Health guidelines on the care and use of laboratory animals. All procedures were approved by the UC Davis Institutional Animal Care and Use Committee.

Non-invasive ACL Rupture

Right hindlimbs underwent ACL injury by tibial compression overload as previously described [26, 27]. Mice were anesthetized via isoflurane inhalation and placed in a prone position with right tibias vertically aligned between two platens for tibial compression. ACL rupture was produced via a single dynamic axial compressive load at 1 mm/s using an electromagnetic materials testing machine (ElectroForce 3200, TA Instruments, New Castle, DE). Buprenorphine analgesia was administered immediately post-injury (0.01 mg/kg). Whole joints were removed for analysis at each time point and fixed in 4% paraformaldehyde for 5–7 days, followed by preservation in 70% ethanol.

Transverse Femoral Fracture

Transverse femoral fractures were produced in right femurs using a modified Einhorn fracture model as previously described [28, 29]. Briefly, mice were given preoperative buprenorphine analgesia and anesthetized via isoflurane inhalation. Stainless steel wires (0.01 inch, Small Parts, Seattle, WA) were surgically inserted into the femoral intramedullary cavity. A blunt load applied perpendicularly to the femur after suture produced consistent and transverse femoral fractures, which were confirmed by radiograph. Buprenorphine (0.01 mg/kg) was administered every 12 hours for 48 hours after injury, and mouse health was monitored daily. Femurs were removed for analysis at each time point and fixed in 4% paraformaldehyde for 5–7 days, followed by preservation in 70% ethanol.

Hindlimb Unloading via Tail Suspension

Immediately after injury, mice were suspended by the base of the tail to undergo HLU for 3, 7, or 14 days (n=5–6/injury/time point). Mice were housed individually in custom tail suspension cages (Techshot, Inc., Greenville, IN) and HLU was performed as previously described [30, 31]. Briefly, cages were prepared with absorbent material underneath wire mesh flooring. Mice were anesthetized and metal loops were attached using cyanoacrylate to tail bases. These loops were then attached to a swivel allowing for 360° rotation and mounted on a bar spanning the length of the cage. Mice were placed at approximately a 30° angle with their heads down, to prevent the hindlimbs from touching the floor of the cage. Mice were able to ambulate freely using their forelimbs, and were given food and water *ad libitum*, as well as nesting materials. Hindlimbs were collected at designated time points and fixed in 4% paraformaldehyde for 5–7 days, followed by preservation in 70% ethanol.

Micro-Computed Tomography (μCT) Analysis of Osteophyte and Fracture Callus Volume

Whole knee joints and femora were scanned using μCT (SCANCO μCT 35, Brüttisellen, Switzerland) to determine total mineralized osteophyte and fracture callus volumes at 14, 21, and 28 days post-injury. Earlier time points were not evaluated using μCT because we

previously found that mineralized osteophytes were not detectable by μCT until at least 2 weeks following non-invasive knee injury [20]. Scans were performed according to rodent bone structure analysis guidelines (X-ray tube potential=55 kVp, intensity=114 μA, 10 μm isotropic nominal voxel size, integration time=900 ms) [32]. The global threshold for "bone" was set equivalent to 567 mg HA/cm^3. Total mineralized osteophyte volume was determined using previously defined methods [20]. Briefly, contours were drawn around all heterotopic mineralized tissue attached to the distal femur and proximal tibia, as well as the entire patella, fabellae, and menisci. The patella, fabellae, and menisci of contralateral limbs were also contoured. Total mineralized osteophyte volume was then determined as the volumetric difference in mineralized tissue between injured and uninjured joints. Results for hindlimb unloaded animals are not shown because no mineralized osteophyte volume was observed by 14 days post-injury. Total mineralized fracture callus volume was also determined using previously defined methods [28, 33]. Contours were drawn around all mineralized tissue down the length of the entire fracture callus, with native cortical bone excluded (Fig. 1A).

Histological Analysis of Chondro/Osteophyte and Fracture Callus Size and Composition

Histology was used to visualize chondro/osteophytes and fracture calluses at all time points. After fixation, knee joints and femora were decalcified using 0.5M EDTA (pH 7.3) until endpoint determination by X-ray (Carestream In vivo FX-MS, Bruker Imaging), and processed for standard paraffin embedding. Sagittal 6 μm sections were cut across the medial knee joint and mid-femur for chondro/osteophyte and fracture callus areas, respectively. Sections were stained with Harris-Modified Hematoxylin and Alcoholic Eosin Y (H&E). Comparable sections (n=1–3/mouse) were selected for analyses, which were performed by three blinded researchers.

Total chondro/osteophyte and fracture callus areas (including fibrous tissue, cartilage, osteoid, and mineralized tissue) were measured at each time point. Chondro/osteophyte areas were quantified as previously described [20]. Briefly, chondro/osteophyte areas were calculated at three locations on the medial compartment of the joint where we have consistently observed osteophyte formation following knee injury: the anterior femur, the anterior horn of the medial meniscus, and the posterior tibia. Fracture callus areas were similarly evaluated at the anterior and posterior aspects of the femur. All areas were quantified using freehand traces in ImageJ (National Institutes of Health, Bethesda, MD) (Fig. 2A, 4A).

Ossification at each time point was evaluated by quantifying ossified tissue areas, including osteoid and mineralized tissue, within chondro/osteophytes and fracture calluses. Ossified tissue was identified as a compact structure with high Eosin content [34]. Total ossified tissue area was normalized by total chondro/osteophyte or fracture callus areas to calculate ossification percentage.

In Vivo Fluorescence Reflectance Imaging (FRI) of Protease Activity

Groups of fractured and ACL ruptured mice subjected to 3 or 7 days of hindlimb unloading or normal cage activity (ground control (GC)) after injury were analyzed for protease activity using *in vivo* FRI (n=4–5/group) as previously described [35]. Briefly, mice were

anesthetized using isoflurane inhalation and injected retro-orbitally with ProSense 750 FAST (PerkinElmer, Waltham, MA) 15 hours prior to imaging. ProSense 750 FAST is a pan-cathepsin fluorescent probe activated by proteases including cathepsins B, L, S, K, V, and D, that are highly active during inflammation [36, 37]. Immediately prior to imaging, mice were anesthetized via isoflurane inhalation and a depilatory was used to remove hair from the ventral aspect of the hindlimbs. Mice were imaged individually in a 13.3 cm field of view in the imaging system (IVIS Spectrum, PerkinElmer, Waltham, MA). The excitation and emission filters were 710±35 nm and 760±35 nm, respectively, based on the peak excitation and emission spectra of the ProSense 750 FAST probe (750 nm and 770 nm, respectively); the exposure time was 15 sec. Care was taken to position mice in similar positions to ensure even epi-illumination across the medial knee and femur for both injured and contralateral limbs. Ankles were taped down and image processing and quantification was performed using the IVIS *Living Image* software.

Fluorescence intensity was quantified as the total radiant efficiency (TRE) ([photons/sec]/[$\mu W/cm^2$]) of the signal within a region of interest (ROI), as previously described [35]. The ROI was a circle of radius 0.35 cm placed over the knee (ACL rupture) or mid-diaphysis of the femur (fracture) on a grayscale photograph of the mice to prevent bias from the fluorescent signal (Fig. 5A).

Quantitative Reverse Transcription Polymerase Chain Reaction (qPCR)

Following FRI, mice were euthanized using CO_2 asphyxiation. Fracture calluses were isolated from fractured mice and the left limbs of uninjured mice (n = 5) as described previously [28]. Muscle was removed from the femur and the bone was cut 2 mm from either end of the callus. Equal lengths of bone were dissected from the femoral diaphyses of uninjured mice. Similarly, whole knee joints were isolated from ACL ruptured mice and the right limbs of uninjured mice (n = 5). Muscles were removed with care to avoid disrupting the joint capsule. The femur was cut 2 mm from the joint to include the distal epiphysis, and the tibia was cut 2 mm from the joint to include the proximal epiphysis. All dissected samples were flash frozen immediately following isolation and processed using TRIzol (Invitrogen, Carlsbad, CA) to isolate RNA according to the manufacturer's protocol. RNA purification was performed using the Qiaquick RNeasy mini-kit (Qiagen, Valencia, CA) and cDNA was generated with the QuantiTect Reverse Transcription Kit (Qiagen).

Quantitative reverse transcription PCR (qPCR) was performed with primer and TaqMan probe sets (Applied Biosystems, Foster City, CA) and the QuantiFast Probe PCR kit (Qiagen) on a Mastercycler Realplex2 (Eppendorf, Westbury, NY). Amplification conditions were 3 min at 95°C, 40 cycles for 3 sec at 95°C, and then 30 sec at 60°C. The following genes were analyzed: interleukin-6 (*IL-6,* Mm00446190_m1), matrix metalloproteinase 13 (MMP-13) (*MMP-13,* Mm00439491_m1), tumor necrosis factor-alpha (TNF-α) (*Tnfa*, Mm00443258_m1), transforming growth factor-beta 1 (TGF-β 1) (*Tgfb-1,* Mm01178820_m1), bone morphogenetic protein-2 (BMP-2) (*Bmp2a*, Mm01340178_m1), BMP-4 (*Bmp-4*, Mm00432087_m1), osteoprotegerin (OPG) (*Opg,* Mm00435454_m1), runt related transcription factor 2 (Runx-2) (*Cbf*, Mm00501584_m1), osteocalcin (OC) (*Bglap*, Mm03413826_mH), and vascular endothelial growth factor (*Vegf*, Mm00437306_m1).

Genes were chosen to examine inflammation (IL-6, TNF-α), bone formation (BMP-2, BMP-4, TGF-β1, OC, Runx-2), bone resorption (OPG, MMP-13), and angiogenesis (VEGF). Results were normalized to beta-actin (*ActB*, Mm00607939_s1) transcript to yield ΔC_t. Results are expressed as $2^{-\Delta Ct}$ [38].

Statistical Analysis

Statistical analyses were used to determine differences between time points within injury groups (ACL rupture or femoral fracture) or ambulation conditions (ground control (GC) or hindlimb unloading (HLU)), as well as differences between groups at each time point. Two-way ANOVA stratified by injury type and time point was used to compare volumes, areas, and ossification of fracture calluses and osteophytes (JMP 11, SAS Institute, Inc., Cary, NC). HLU mice were compared to GC mice using three-way ANOVA stratified by injury type, ambulation condition, and time point. FRI results were analyzed using a four-way mixed design ANOVA stratified by injury type, time point, ambulation (GC or HLU), and limb (injured or contralateral) as a within-subjects variable. qPCR results were analyzed for differences within each injury type using two-way ANOVAs stratified by time point and ambulation. Post hoc analyses were carried out by the Tukey-Kramer test. All data is presented as mean ± standard deviation. Significance was defined as $p<0.05$ for all tests.

Results

MicroCT Analysis of Mineralized Osteophyte and Fracture Callus Volumes

In general, formation and mineralization of fracture calluses occurred at earlier time points than for osteophytes (Fig. 1). Osteophyte volume increased linearly by 9.5-fold between day 14 and day 28, whereas mineralized fracture callus volume did not change significantly within the same time frame (Fig. 1B). A significant interaction between time point and injury was found, indicating that the time course of osteophyte formation was different from that of fracture callus formation ($p=0.0375$). Fracture calluses were larger than osteophytes at all time points ($p<0.0001$) (Fig. 1A, 1B). The effect of injury on tissue mineral density (TMD) was also shown to vary by time point, with fracture callus TMD increasing over time, and osteophyte TMD remaining constant ($p=0.0017$) (Fig. 1C).

Histological Analysis of Chondro/Osteophyte and Fracture Callus Size and Ossification

Histological analysis similarly showed that, while both osteophyte and fracture callus formation began at early time points after injury, fracture callus growth and ossification occurred earlier than that of osteophytes (Fig. 2). Fracture callus area increased relatively linearly between days 3 (3.27 mm^2) and 14 post-injury (10.30 mm^2), an overall 3-fold increase in callus area. Fracture callus area then decreased by 39% after 21 days of injury and maintained size until the end of the experiment (Fig. 2B). Osteophytes, on the other hand, exhibited linear growth between days 7 (0.33 mm^2) and 21 (1.59 mm^2), an overall 5-fold increase in area. Osteophyte area then remained constant between days 21 and 28 after injury (Fig. 2B). A significant interaction of injury and time point was observed, indicating that the two structures exhibited different growth patterns over time ($p=0.0002$). Total osteophyte area was significantly less than total fracture callus area at each time point ($p<0.0001$) (Fig. 2B).

Osteophytes and fracture calluses also exhibited differences in the rate of ossification. Fracture callus ossification increased at early time points, from 0% at day 3 to 18% at day 5. Ossification continued to increase until it plateaued after day 21 (Fig. 2C). Osteophytes, on the other hand, remained primarily cartilaginous until day 14 (7 %), after which ossification increased throughout the duration of the experiment. By day 28, osteophyte ossification was 42% (Fig. 2C). Osteophyte ossification percentage was significantly less than fracture callus ossification percentage at all time points except day 3 ($p<0.0001$) (Fig. 2C).

Histological Analysis of Fracture Callus and Osteophyte Formation and Maturation

Histological assessment revealed that both fracture calluses and osteophytes achieved similar developmental milestones, but on slightly different time scales (Fig. 3). Inflammation dominated the injury response 3 days following both types of injury, manifesting as a robust thickening of the periosteum and synovium in fractured and ACL ruptured mice, respectively. Blood clotting was also observed in fractured femora. However, the similarities in the time course of cellular responses for each injury type begin diverging by day 5. After fracture, robust cartilage differentiation from precursor cells was observed after 5 days, with intramembranous bone formation proceeding distal to the break. New periosteum was observed around the perimeter of the callus. In contrast, 5 days post-ACL rupture, cartilage condensation was not significantly underway, though the periosteal/synovial reaction and intramembranous bone formation at the joint margins continued. By day 7 after injury, fractured femora demonstrated a strong chondrogenic response, with intramembranous bone formation at the periphery of the callus, and vascular invasion of the interior of the callus (Fig. 3). In contrast, at 7 days post-ACL rupture, intramembranous bone formation was just beginning at the edges of the joint capsule, and chondrogenesis/fibrous tissue formation was starting in the areas around the meniscus.

At later time points, the healing process after fracture was dominated by bone formation. By day 14 after fracture, the cartilaginous callus was mature, with osteogenesis as the primary metabolic response (Fig. 3). However, ACL injury at the same time point was only just demonstrating early chondrophyte formation via robust chondrogenesis at the joint margins, and fibrous cartilage in the joint capsule (Fig. 3). Additionally, we observed hypertrophic meniscal chondrocytes and gradual ossification of the anterior horn of the medial meniscus. By day 21 after fracture, the cartilaginous callus template was nearly completely replaced by bone, with a robust osteogenic response, and the original cortical bone had started the remodeling process. In contrast, ACL ruptured joints after 21 days had formed chondrophytes at joint margins, with very little osteogenesis apparent. By day 28 after fracture, the fracture calluses had begun remodeling and restoring the morphological features of normal, intact bone. In contrast, chondro/osteophytes were continuing chondrogenesis at this stage, still with little osteogenesis.

Effect of HLU on Chondro/Osteophyte and Fracture Callus Growth

As expected, HLU significantly inhibited both fracture callus and osteophyte formation. MicroCT results indicated that at 14 days post-fracture, the average mineralized fracture callus volume for HLU mice was 60% less than GC mice at the same time point ($p=0.0098$).

Mineralized osteophytes were not observed 14 days after ACL injury in either HLU or GC mice.

Assessment of histological sections further indicated that HLU inhibited both fracture callus and chondro/osteophyte size (Fig. 4). Fracture callus area was 32% and 55% less in hindlimb unloaded mice compared to GC mice after 7 and 14 days of tail suspension, respectively. Chondro/osteophyte area was not significantly different between HLU and GC mice 7 days after injury, but HLU mice exhibited 68% less chondro/osteophyte area than GC mice after 14 days ($p=0.0009$) (Fig. 4B). Qualitative histological examination revealed a clear reduction in inflammation, indicated by a lack of periosteal and synovial thickening, cell infiltration, and chondrogenesis in HLU mice (Fig. 3). Knee joints from HLU mice after ACL injury similarly demonstrated less cellular expansion in the synovium, less swelling, and, by day 14, reduced chondrogenesis compared to GC mice after ACL injury (Fig. 3).

In Vivo Fluorescence Reflectance Imaging (FRI) of Protease Activity

FRI analysis of mice indicated that both femur fracture and ACL rupture initiated considerable inflammation and protease activity by 3 and 7 days post-injury (Fig. 5). Total radiant efficiency (TRE) in GC mice was 103% and 79% higher in fractured and ACL ruptured limbs than in paired contralateral limbs at day 3, respectively. Similar differences were observed at day 7 for GC mice, with 102% and 57% higher TRE in fractured and ACL ruptured limbs, respectively. HLU resulted in reduced protease activity in injured limbs when compared to GC ($p=0.0007$), with a more marked effect after ACL rupture than after fracture. HLU after ACL rupture led to a significant 44% and 41% lower TRE compared to injured GC limbs after 3 and 7 days, respectively. HLU after fracture exhibited a 26% and 25% lower TRE compared to injured GC limbs after 3 and 7 days, respectively, indicating a trend, but not a statistically significant difference. Mice subjected to HLU after ACL rupture did not exhibit significant differences in TRE between injured and contralateral limbs, while fractured mice subjected to HLU still exhibited 81% and 102% greater TRE in injured limbs at days 3 and 7, respectively. No significant differences were observed between contralateral limbs due to injury type or ambulation condition.

Gene Expression in Fracture Calluses and Injured Knees

Both bone fracture and ACL rupture led to time point-dependent changes in gene expression by 3 and 7 days after injury, though gene expression was altered considerably more in fractured femurs than in injured knees. In fractured femurs, several genes were elevated in fracture calluses compared to uninjured femurs at 7 days post-fracture, including IL-6 (147-fold), BMP-2 (6-fold), OC (3-fold), Runx-2 (7-fold), OPG (21-fold), MMP-13 (45-fold), and VEGF (5-fold), indicating a complex healing process coordinated by inflammatory, bone formation and resorption, and angiogenic responses (Fig. 6). OPG was also elevated 16-fold compared to uninjured femurs at day 3 post-fracture (Fig. 6), indicating early osteogenic differentiation after injury. In contrast, in ACL ruptured knees, only OC and VEGF levels were elevated compared to uninjured knees; both were elevated greater than 1,000-fold at both day 3 and day 7 post-injury (Fig. 6). No significant differences were observed for TNF-α or TGF-β1 expression for either injury type.

HLU also led to changes in gene expression after both fracture and ACL rupture (Fig. 6). For example, IL-6 was significantly upregulated (182-fold) after 3 days of HLU with fracture compared to GC mice. In contrast, IL-6 expression was lower in ACL injured HLU mice compared to GC mice at both day 3 and day 7, though these differences were not statistically significant. In fractured mice, main effects of ambulation (GC or HLU) were also observed for BMP-2, OC, Runx-2, OPG, MMP-13, and VEGF. For ACL ruptured mice, main effects of ambulation (GC or HLU) were observed for OC, OPG, and VEGF (Fig. 6).

Discussion

In this study, we drew parallels between osteophyte and fracture callus formation. Both structures showed evidence of early intramembranous bone formation, followed by robust endochondral bone formation with a cartilaginous template. However, fracture callus growth and ossification occurred earlier than osteophyte formation, with hard fracture callus growth plateauing after 14 days, when osteophyte growth was just beginning to increase. Hindlimb unloading following injury led to considerable decreases in osteophyte and fracture callus size; HLU also resulted in decreased inflammation and protease activity in injured limbs detected with FRI, particularly following ACL rupture. These data indicate that chondro/osteophytes and fracture calluses both experience similar milestones during formation, though on different time scales, and that both structures are affected by their mechanical environment. qPCR analysis of fracture calluses revealed a robust cellular response, including increases in inflammatory, bone formation and resorption, and angiogenic factors compared to uninjured controls, while ACL ruptured knees exhibited a much more muted response, with increases in OC and VEGF levels only. These results are contrary to our initial hypotheses that fracture calluses and osteophytes form via similar inflammatory, anabolic, and catabolic pathways. These data may also suggest that HLU affects osteophyte and fracture callus size by different mechanisms.

Previous studies have examined developmental stages of both fracture calluses and osteophytes. During fracture healing, mesenchymal cells migrate to the damage site and differentiate into chondrocytes, osteoblasts, or fibroblasts depending on the local mechanics [39]. These cells then lay down extracellular matrix corresponding to their cell type. In early stages following injury, woven bone is laid down at the margins of the growing callus via intramembranous ossification and cartilage is produced in the callus center. Later, endochondral ossification transforms the cartilaginous template into bone, which gradually remodels [39, 40]. Osteophyte formation also begins with chondrogenic differentiation of mesenchymal progenitor cells, followed by the development of fibrocartilage and a cartilaginous template (chondrophytes). Additionally, osteophytes display both endochondral ossification in the inner core of the osteophyte, and intramembranous ossification at the periphery [4, 13]. However, while fracture callus remodeling to native bone morphology is well established, previous studies have shown osteophytes to continue increasing in size through time points as late as 8 weeks after injury [15, 20, 27]. Remodeling has not been demonstrated in osteophytes, and during this time course, we did not observe any statistical reduction in osteophyte size suggestive of remodeling. We speculate that there would be no significant remodeling of osteophytes at later time points, which would be consistent with other studies [27]. These previous studies suggest that there

are similarities between fracture callus and osteophyte development, but comparisons are limited because most previous studies examining osteophyte growth have been performed using human samples.

In our study, we used a noninvasive mouse model of PTOA, allowing us to examine osteophyte formation throughout the full time course of OA development after ACL rupture. Osteophytes are typically examined in isolation, but in this study, we also examined the margins around the articular surfaces and the periphery of the joint. During fracture repair, intramembranous bone formation begins distally and forms in the direction of the injury. We observed the same occurrence in our ACL injured joints, with the articular cartilage and growth plate cartilage cell types serving as boundaries for intramembranous bone formation. We were thus able to identify an additional morphological similarity between fracture repair and osteophyte formation.

Fracture callus and osteophyte development have both been shown to be sensitive to local biomechanics after injury [9, 14, 39, 41–44]. Previous studies have observed decreased osteophyte formation after unloading in a guinea pig model of chemically-induced OA, and decreased fracture callus growth in a rat tibial fracture model [6, 7, 24]. Our results agree with these studies, and suggest that loading from normal ambulation influences both osteophyte and fracture callus formation. Tail suspension has been shown to decrease blood perfusion to hindlimbs, and angiogenic factors have been shown to combat the HLU-induced reduction in osteogenesis which may indirectly impact inflammation in hindlimbs, consequently affecting fracture callus and osteophyte formation [24, 45]. While our FRI results do suggest that HLU leads to decreased protease activity and inflammation after both fracture and ACL rupture, the exact mechanism may differ by injury type. VEGF levels were elevated compared to uninjured controls after both fracture and ACL rupture, but HLU did not appear to affect expression at either time point. Furthermore, the mechanism relating protease activity to inflammation is unclear. We found that IL-6 levels after fracture increased significantly after 3 days of HLU, a similar finding to a previous study in which rat tail suspension induced IL-6 secretion after 5 days of unloading [46]. Conversely, we observed non-significant decreases in IL-6 expression during HLU in ACL ruptured mice. IL-6 has been found to modulate cathepsins B and L [47, 48], but how that may translate to the decreased inflammation observed with FRI in this study remains unclear. TNF-α, MMP-13, and TGF-β1, the other inflammatory mediators investigated in this study, did not show any variation due to HLU for either injury type, suggesting that other pathways may be responsible for the decrease in inflammation observed with FRI.

While HLU led to decreased inflammation detected by FRI in both injury types, it also led to decreases in OPG and OC after 7 days of unloading post-ACL rupture compared to GC mice. These results may indicate that HLU leads to an increase in osteoclast activity along with a decrease in osteoblast activity, which corresponds with the observed decrease in osteophyte formation. These results agree with previous work showing decreased osteoblast differentiation and increased bone resorption with HLU [46]. GC mice exhibited robust upregulation of OC compared to uninjured mice, unlike OPG, suggesting that OC, and not OPG, may be an important biological factor in osteophyte formation. However, one limitation of this study is that qPCR was performed on whole joint samples, therefore OC

upregulation may be due to changes in other joint tissues. Despite this limitation, previous work has observed high levels of OC in osteophytic articular chondrocytes [49]. Further studies investigating the role of OC on osteophyte formation are needed.

Several limitations of this study must be taken into consideration when interpreting the results. First, we used histology to examine fracture callus and osteophyte growth. Fracture calluses and osteophytes are three-dimensional structures, and so two-dimensional histology allows limited quantification of their growth. In this study, sections from similar locations in the joint or femur were chosen for comparison, but slight differences in the selection may have caused some variability in the data. Manually drawing areas for chondro/osteophytes and fracture calluses was also somewhat subjective to the individual performing the analysis. We circumvented these issues by having three blinded researchers perform the analyses, and instructed them to include all fibrous tissue encapsulating growing chondro/osteophytes and fracture calluses, as the surrounding tissues were not always distinguishable from the actual structures themselves. Statistical analyses confirmed that there was no significant variation between researchers at each time point for both injury types. Additionally, our identification of intramembranous bone formation may have been hindered by the time points selected for analysis. We identified intramembranous bone formation as ossified areas in locations without an observable cartilage template (as would be seen in endochondral ossification), but it is unclear if these areas were previously cartilaginous. Despite this limitation, our observations of intramembranous bone formation are consistent with previous work that has identified intramembranous ossification in similar locations in both osteophytes and fracture calluses [3, 4, 14]. Furthermore, qPCR and FRI were performed at the same time points for both injury types (days 3 and 7 post-injury), when our histology indicates that calluses and osteophytes are in different developmental stages at 3 and 7 days post-injury. This may partially explain why qPCR of fracture calluses showed a robust adaptive response, with a comparatively small response following ACL rupture. This may limit our ability to compare qPCR results across injury types, though we were still able to provide insight into the effect of unloading on gene expression profiles. Finally, fractures induced by the Einhorn method are stabilized with an intramedullary pin, while the ACL injured joint was stabilized only by other joint tissues. Both of these methods likely resulted in some instability of the bone/joint, though it is impossible to directly compare the two. Previous studies examining non-stabilized fractures have shown that the level of stability can affect gene expression and the time course of healing [50, 51]. We used the Einhorn model because it is consistent, well-established, and well-characterized. However, we did not examine or control for mechanical changes after fracture or ACL rupture, which may have accounted for the differences in size and time scale of callus and osteophyte formation. Despite this limitation, general trends in fracture callus and osteophyte formation were still comparable.

Despite the prevalence of osteophytes during OA, relatively little is known regarding the mechanical and biological factors that influence their formation. In this study, we aimed to increase scientific understanding of osteophyte formation during PTOA by drawing comparisons with fracture callus formation. Our results suggest that, while osteophytes and fracture calluses share developmental milestones, the time course and mechanism of formation of these structures are somewhat different. Increasing scientific knowledge of

osteophyte formation may translate to clinical treatments for osteophytes and other instances of ectopic bone formation.

Acknowledgments

Research reported in this publication was supported by the National Institute of Arthritis and Musculoskeletal and Skin Diseases, part of the National Institutes of Health, under Award Number AR062603. The content is solely the responsibility of the authors and does not necessarily represent the official views of the National Institutes of Health. The funding body was not involved with design, collection, analysis, or interpretation of data; or in the writing of the manuscript. The authors have no conflicts of interest to disclose.

References

1. Lawrence RC, Felson DT, Helmick CG, et al. Estimates of the prevalence of arthritis and other rheumatic conditions in the United States. Part II. Arthritis Rheum. 2008; 58(1):26–35. [PubMed: 18163497]
2. Goldring SR, Goldring MB. Clinical aspects, pathology and pathophysiology of osteoarthritis. J Musculoskelet Neuronal Interact. 2006; 6(4):376–378. [PubMed: 17185832]
3. van der Kraan PM, van den Berg WB. Osteophytes: relevance and biology. Osteoarthritis Cartilage. 2007; 15(3):237–244. [PubMed: 17204437]
4. Zoricic S, Maric I, Bobinac D, Vukicevic S. Expression of bone morphogenetic proteins and cartilage-derived morphogenetic proteins during osteophyte formation in humans. J Anat. 2003; 202(Pt 3):269–277. [PubMed: 12713267]
5. Williams JM, Brandt KD. Exercise increases osteophyte formation and diminishes fibrillation following chemically induced articular cartilage injury. J Anat. 1984; 139(Pt 4):599–611. [PubMed: 6526713]
6. Williams JM, Brandt KD. Temporary immobilisation facilitates repair of chemically induced articular cartilage injury. J Anat. 1984; 138(Pt 3):435–446. [PubMed: 6735906]
7. Williams JM, Brandt KD. Immobilization ameliorates chemically-induced articular cartilage damage. Arthritis Rheum. 1984; 27(2):208–216. [PubMed: 6696774]
8. Palmoski MJ, Brandt KD. Immobilization of the knee prevents osteoarthritis after anterior cruciate ligament transection. Arthritis Rheum. 1982; 25(10):1201–1208. [PubMed: 7138593]
9. Murata K, Kokubun T, Morishita Y, et al. Controlling Abnormal Joint Movement Inhibits Response of Osteophyte Formation. Cartilage. 2017 1947603517700955.
10. Bakker AC, van de Loo FA, van Beuningen HM, et al. Overexpression of active TGF-beta-1 in the murine knee joint: evidence for synovial-layer-dependent chondro-osteophyte formation. Osteoarthritis Cartilage. 2001; 9(2):128–136. [PubMed: 11237660]
11. Scharstuhl A, Vitters EL, van der Kraan PM, van den Berg WB. Reduction of osteophyte formation and synovial thickening by adenoviral overexpression of transforming growth factor beta/bone morphogenetic protein inhibitors during experimental osteoarthritis. Arthritis Rheum. 2003; 48(12):3442–3451. [PubMed: 14673995]
12. Matyas JR, Sandell LJ, Adams ME. Gene expression of type II collagens in chondro-osteophytes in experimental osteoarthritis. Osteoarthritis Cartilage. 1997; 5(2):99–105. [PubMed: 9135821]
13. Gelse K, Soder S, Eger W, et al. Osteophyte development--molecular characterization of differentiation stages. Osteoarthritis Cartilage. 2003; 11(2):141–148. [PubMed: 12554130]
14. Marsell R, Einhorn TA. The biology of fracture healing. Injury. 2011; 42(6):551–555. [PubMed: 21489527]
15. Einhorn TA. The cell and molecular biology of fracture healing. Clin Orthop Relat Res. 1998; 355(Suppl):S7–21.
16. Bostrom MP, Asnis P. Transforming growth factor beta in fracture repair. Clin Orthop Relat Res. 1998; 355(Suppl):S124–131.
17. Puddu G, Cipolla M, Cerullo G, Scala A. Arthroscopic treatment of the flexed arthritic knee in active middle-aged patients. Knee Surg Sports Traumatol Arthrosc. 1994; 2(2):73–75. [PubMed: 7584187]

18. Ritter MA, Harty LD, Davis KE, et al. Predicting range of motion after total knee arthroplasty. Clustering, log-linear regression, and regression tree analysis. J Bone Joint Surg Am. 2003; 85-A(7):1278–1285. [PubMed: 12851353]
19. Pottenger LA, Phillips FM, Draganich LF. The effect of marginal osteophytes on reduction of varus-valgus instability in osteoarthritic knees. Arthritis Rheum. 1990; 33(6):853–858. [PubMed: 2363739]
20. Hsia AW, Anderson MJ, Heffner MA, et al. Osteophyte formation after ACL rupture in mice is associated with joint restabilization and loss of range of motion. J Orthop Res. 2017; 35(3):466–473. [PubMed: 27031945]
21. Gerstenfeld LC, Cullinane DM, Barnes GL, et al. Fracture healing as a post-natal developmental process: molecular, spatial, and temporal aspects of its regulation. J Cell Biochem. 2003; 88(5): 873–884. [PubMed: 12616527]
22. Hiltunen A, Vuorio E, Aro HT. A standardized experimental fracture in the mouse tibia. J Orthop Res. 1993; 11(2):305–312. [PubMed: 8483044]
23. Ekeland A, Engesaeter LB, Langeland N. Mechanical properties of fractured and intact rat femora evaluated by bending, torsional and tensile tests. Acta Orthop Scand. 1981; 52(6):605–613. [PubMed: 7331797]
24. Matsumoto T, Sato S. Stimulating angiogenesis mitigates the unloading-induced reduction in osteogenesis in early-stage bone repair in rats. Physiol Rep. 2015; 3(3)
25. Jilka RL. The relevance of mouse models for investigating age-related bone loss in humans. J Gerontol A Biol Sci Med Sci. 2013; 68(10):1209–1217. [PubMed: 23689830]
26. Lockwood KA, Chu BT, Anderson MJ, et al. Comparison of loading rate-dependent injury modes in a murine model of post-traumatic osteoarthritis. J Orthop Res. 2014; 32(1):79–88. [PubMed: 24019199]
27. Christiansen BA, Anderson MJ, Lee CA, et al. Musculoskeletal changes following non-invasive knee injury using a novel mouse model of post-traumatic osteoarthritis. Osteoarthritis Cartilage. 2012; 20(7):773–782. [PubMed: 22531459]
28. Toupadakis CA, Wong A, Genetos DC, et al. Long-term administration of AMD3100, an antagonist of SDF-1/CXCR4 signaling, alters fracture repair. J Orthop Res. 2012; 30(11):1853–1859. [PubMed: 22592891]
29. Bonnarens F, Einhorn TA. Production of a standard closed fracture in laboratory animal bone. J Orthop Res. 1984; 2(1):97–101. [PubMed: 6491805]
30. Warden SJ, Galley MR, Richard JS, et al. Reduced gravitational loading does not account for the skeletal effect of botulinum toxin-induced muscle inhibition suggesting a direct effect of muscle on bone. Bone. 2013; 54(1):98–105. [PubMed: 23388417]
31. Anderson MJ, Diko S, Baehr LM, et al. Contribution of mechanical unloading to trabecular bone loss following non-invasive knee injury in mice. J Orthop Res. 2016
32. Bouxsein ML, Boyd SK, Christiansen BA, et al. Guidelines for assessment of bone microstructure in rodents using micro-computed tomography. J Bone Miner Res. 2010; 25(7):1468–1486. [PubMed: 20533309]
33. Morgan EF, Mason ZD, Chien KB, et al. Micro-computed tomography assessment of fracture healing: relationships among callus structure, composition, and mechanical function. Bone. 2009; 44(2):335–344. [PubMed: 19013264]
34. Rentsch C, Schneiders W, Manthey S, et al. Comprehensive histological evaluation of bone implants. Biomatter. 2014:4.
35. Satkunananthan PB, Anderson MJ, De Jesus NM, et al. In vivo fluorescence reflectance imaging of protease activity in a mouse model of post-traumatic osteoarthritis. Osteoarthritis Cartilage. 2014; 22(10):1461–1469. [PubMed: 25278057]
36. Conus S, Simon HU. Cathepsins: key modulators of cell death and inflammatory responses. Biochem Pharmacol. 2008; 76(11):1374–1382. [PubMed: 18762176]
37. Goergen CJ, Azuma J, Barr KN, et al. Influences of aortic motion and curvature on vessel expansion in murine experimental aneurysms. Arterioscler Thromb Vasc Biol. 2011; 31(2):270–279. [PubMed: 21071686]

38. Schmittgen TD, Livak KJ. Analyzing real-time PCR data by the comparative C(T) method. Nat Protoc. 2008; 3(6):1101–1108. [PubMed: 18546601]
39. Doblare M, Garcia JM, Gomez MJ. Modelling bone tissue fracture and healing: a review. Engineering Fracture Mechanics. 2004; 71(13–14):1809–1840.
40. Carter DR, Beaupre GS, Giori NJ, Helms JA. Mechanobiology of skeletal regeneration. Clinical Orthopaedics and Related Research. 1998; (355):S41–S55. [PubMed: 9917625]
41. Augat P, Simon U, Liedert A, Claes L. Mechanics and mechano-biology of fracture healing in normal and osteoporotic bone. Osteoporos Int. 2005; 16(Suppl 2):S36–43. [PubMed: 15372141]
42. Buckland-Wright JC, Macfarlane DG, Lynch JA. Osteophytes in the osteoarthritic hand: their incidence, size, distribution, and progression. Ann Rheum Dis. 1991; 50(9):627–630. [PubMed: 1929585]
43. Felson DT, Gale DR, Elon Gale M, et al. Osteophytes and progression of knee osteoarthritis. Rheumatology (Oxford). 2005; 44(1):100–104. [PubMed: 15381791]
44. Sellam J, Berenbaum F. The role of synovitis in pathophysiology and clinical symptoms of osteoarthritis. Nat Rev Rheumatol. 2010; 6(11):625–635. [PubMed: 20924410]
45. Colleran PN, Wilkerson MK, Bloomfield SA, et al. Alterations in skeletal perfusion with simulated microgravity: a possible mechanism for bone remodeling. J Appl Physiol (1985). 2000; 89(3): 1046–1054. [PubMed: 10956349]
46. Grano M, Mori G, Minielli V, et al. Rat hindlimb unloading by tail suspension reduces osteoblast differentiation, induces IL-6 secretion, and increases bone resorption in ex vivo cultures. Calcif Tissue Int. 2002; 70(3):176–185. [PubMed: 11907715]
47. Gerber A, Welte T, Ansorge S, Buhling F. Expression of cathepsins B and L in human lung epithelial cells is regulated by cytokines. Adv Exp Med Biol. 2000; 477:287–292. [PubMed: 10849756]
48. Gerber A, Wille A, Welte T, et al. Interleukin-6 and transforming growth factor-beta 1 control expression of cathepsins B and L in human lung epithelial cells. J Interferon Cytokine Res. 2001; 21(1):11–19. [PubMed: 11177576]
49. Gelse K, Ekici AB, Cipa F, et al. Molecular differentiation between osteophytic and articular cartilage--clues for a transient and permanent chondrocyte phenotype. Osteoarthritis Cartilage. 2012; 20(2):162–171. [PubMed: 22209871]
50. Le AX, Miclau T, Hu D, Helms JA. Molecular aspects of healing in stabilized and non-stabilized fractures. J Orthop Res. 2001; 19(1):78–84. [PubMed: 11332624]
51. Histing T, Heerschop K, Klein M, et al. Characterization of the healing process in non-stabilized and stabilized femur fractures in mice. Arch Orthop Trauma Surg. 2016; 136(2):203–211. [PubMed: 26602903]

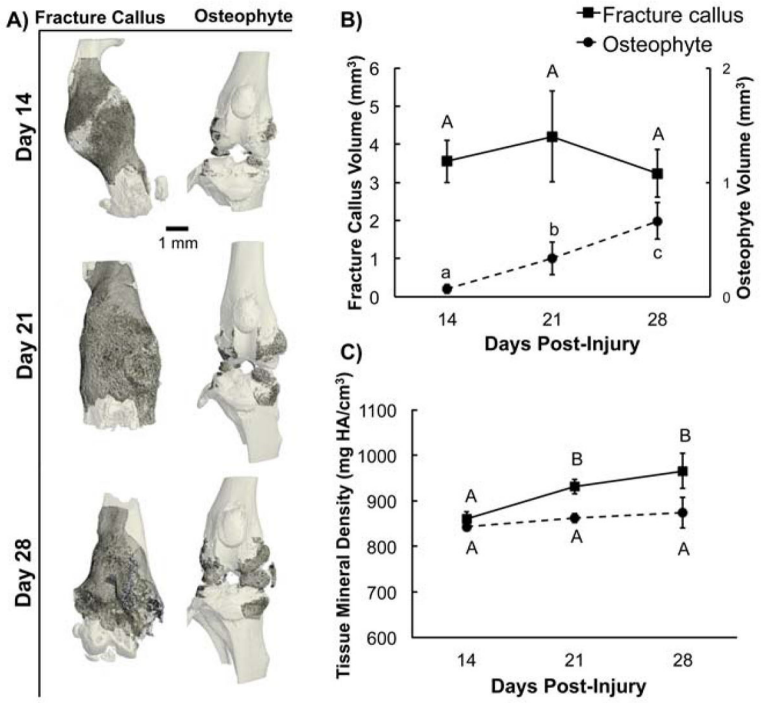

Figure 1. MicroCT analysis of fracture calluses and ACL ruptured joints

(A) Three-dimensional μCT renderings of fracture calluses (left) and osteophytes (right). Callus and osteophyte volume depicted in dark grey, native bone in light grey. (B) Osteophyte and fracture callus volume at days 14, 21, and 28 after injury. Mineralized fracture callus volume remained statistically similar at each time point, while osteophyte volume increased over time ($p<0.0001$). A significant interaction between time point and injury type indicated differences in trajectory for fracture callus and osteophyte growth ($p=0.0375$). (C) Osteophyte and fracture callus bone tissue mineral density (TMD) at days 14, 21, and 28 after injury. Fracture callus TMD increased significantly over time, while osteophyte TMD did not change ($p=0.0017$). Time points that do not share a letter are significantly different from each other ($p<0.05$). Data is presented as mean ± SD.

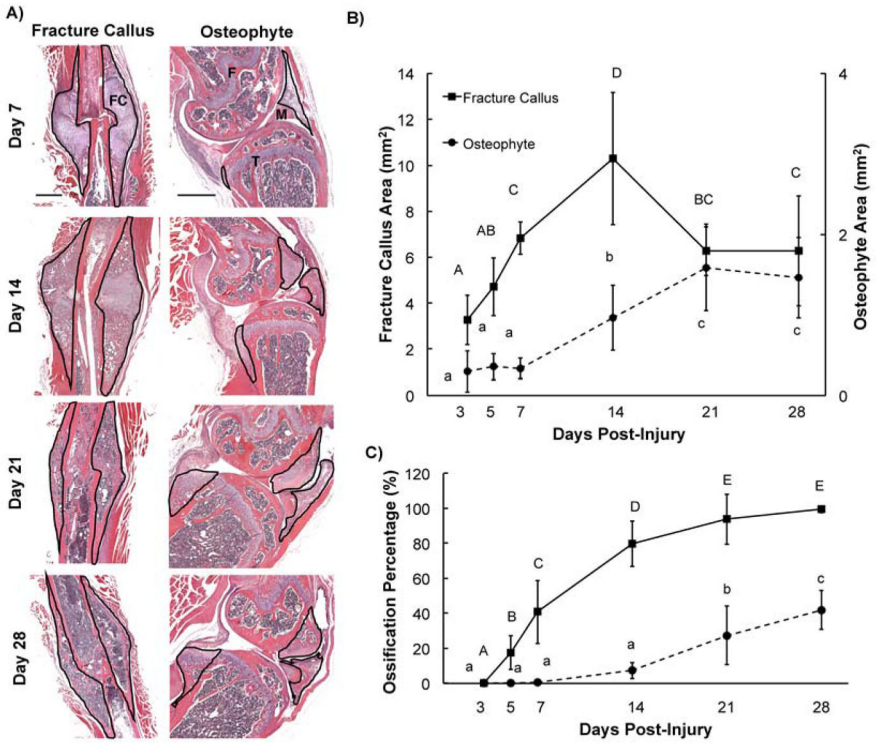

Figure 2. Histological assessment of osteophyte and fracture callus size and ossification

(A) Representative H&E stained images for fracture calluses and chondro/osteophytes at 7, 14, 21, and 28 days post-injury (FC= fracture callus; F= femur; M= meniscus; T= tibia). Scale bar is 1 mm. Fracture callus and chondro/osteophyte areas outlined in black. (B) Fracture callus and chondro/osteophyte areas as a function of days after injury. Fracture callus growth occurred at earlier time points, with remodeling and a subsequent decrease in area at later time points. Osteophyte growth occurred at comparatively later time points, but continued throughout the duration of the experiment. A significant interaction between time point and injury type indicates statistical differences in growth trend ($p=0.0002$). (C) Ossification percentage for fracture calluses and chondro/osteophytes over time. Fracture calluses exhibit earlier ossification, eventually plateauing by days 21–28. Osteophyte ossification continuously increased started at day 14 after injury. Time points that do not share a letter are significantly different from each other ($p<0.05$). Data is presented as mean ± SD.

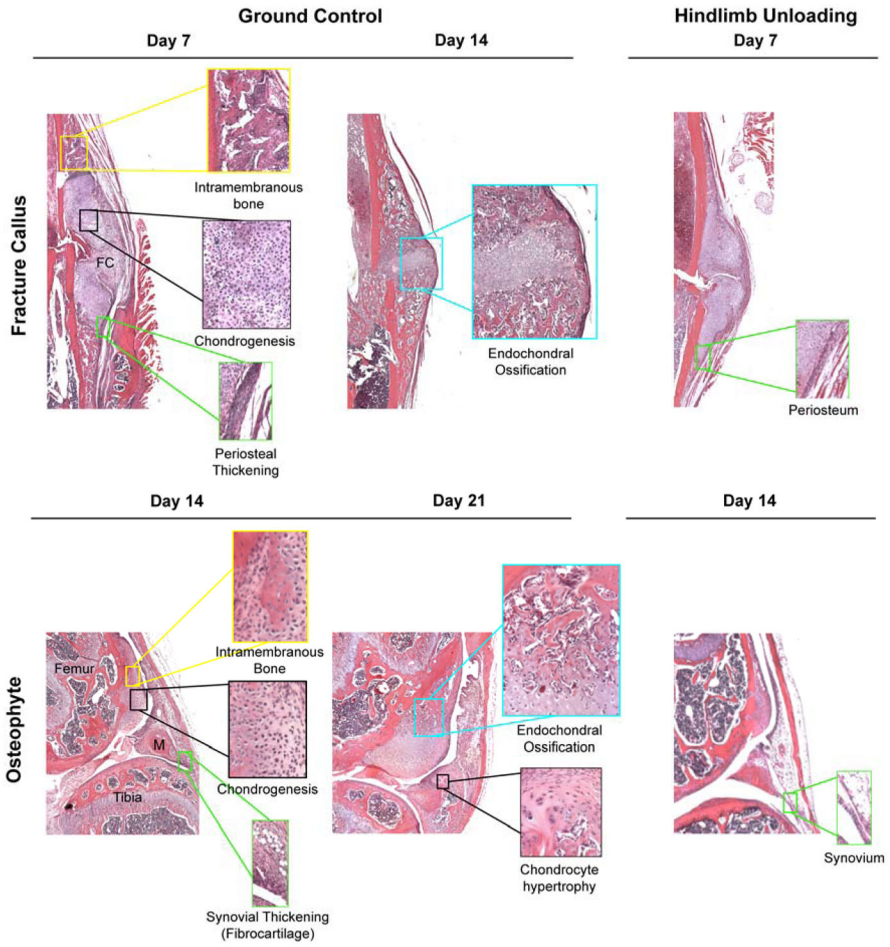

Figure 3. Histological comparison of fracture callus and osteophyte composition

Representative H&E stained images for fracture calluses (ground control days 7 and 14, hindlimb unloaded day 7) and osteophytes (days 14 and 21, hindlimb unloaded day 14). Both fracture calluses and osteophytes exhibited similar milestone stages of fracture healing, but at different time points. Fracture calluses exhibited robust chondrogenesis and intramembranous bone formation at day 7, similar to osteophyte composition at day 14. Similarly, fracture calluses underwent endochondral ossification by day 14, while osteophyte endochondral ossification did not occur until day 21. ACL ruptured GC mice exhibited fibrocartilaginous thickening of the synovium and chondrocyte hypertrophy in the meniscus by 14 days post-injury. HLU limbs exhibited decreased inflammation, including reduced periosteal and synovial thickening for fractured and ACL ruptured limbs, respectively, as well as reduced cell infiltration via the periosteum and synovium.

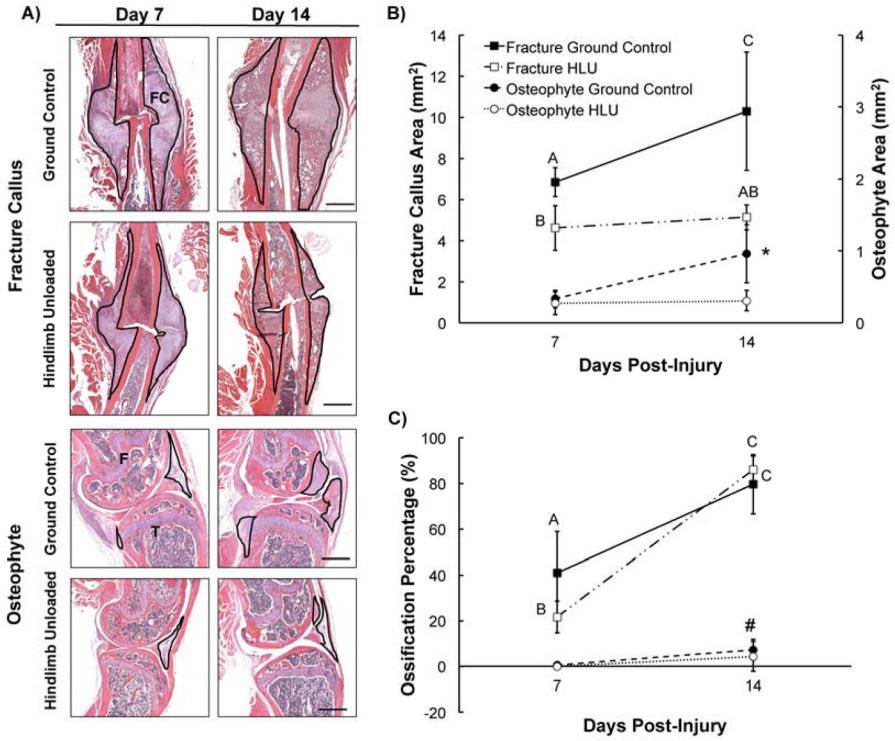

Figure 4. Reduced osteophyte formation in unloaded injured hindlimbs

(A) Representative H&E stained images for ground control (GC) and hindlimb unloaded (HLU) chondro/osteophytes and fracture calluses 7 and 14 days after injury (F = femur, T = tibia, FC = fracture callus). Osteophyte and fracture callus areas outlined in black. Scale bar = 1 mm. (B) HLU reduced osteophyte and fracture callus size. HLU fracture callus areas were not significantly different between time points, but were significantly less than ground control callus areas at each time point ($p=0.0077$). Similarly, HLU chondro/osteophyte areas were not significantly different at each time point, but were significantly lower than ground control areas at day 14 ($p=0.0009$). Fracture callus data not connected by the same letter are significantly different. Asterisk indicates that osteophyte area for GC mice at day 14 is significantly greater than all other ACL rupture groups. (C) HLU affected ossification percentage in fracture calluses, but not osteophytes. HLU fracture calluses were significantly lower in ossification percentage at day 7 compared to GC calluses, but the two groups were not significantly different by day 14 ($p=0.0042$). Conversely, HLU did not affect ossification percentage for osteophytes. Fracture callus data not connected by the same letter are significantly different. # indicates that osteophyte ossification percentages varied by time point ($p<0.0001$). Both area and ossification percentage were significantly different depending on injury type ($p<0.0001$). Data is presented as mean ± SD.

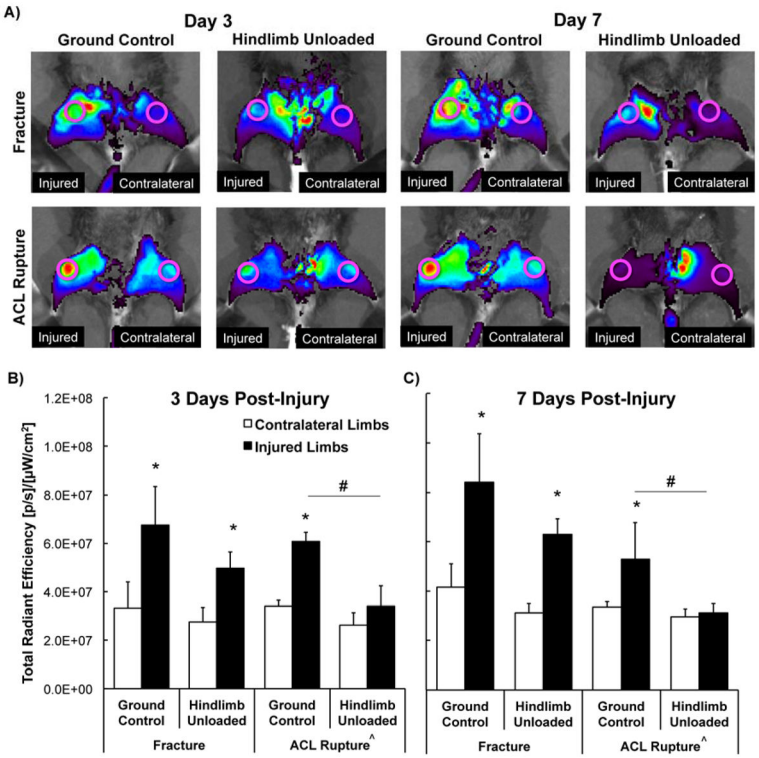

Figure 5. Decreased inflammatory protease activity in unloaded injured limbs

(A) Representative FRI images of ground control (GC) and hindlimb unloaded (HLU) limbs at days 3 and 7 after fracture or ACL rupture. Pink circles represent regions of interest for analysis. (B-C) Total radiant efficiency for injured and contralateral limbs for each injury type after 3 and 7 days of either normal ambulation or hindlimb unloading. HLU reduced inflammation and protease activity in injured limbs, particularly in ACL ruptured mice. * indicates total radiant efficiency of injured limbs is significantly greater than that of paired contralateral limbs. # indicates HLU injured limbs differed from GC injured limbs. ^ indicates injured limbs differ by injury type ($p<0.0001$).

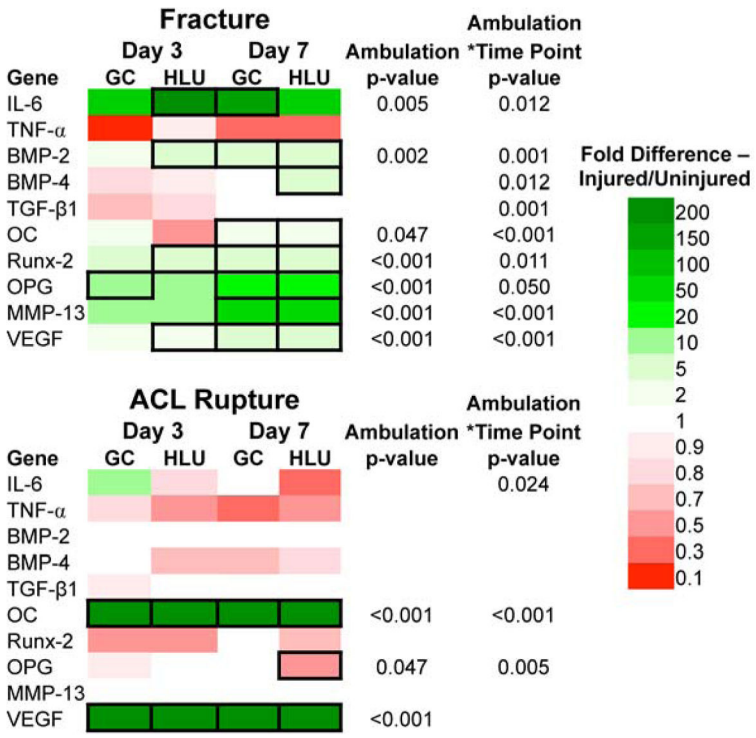

Figure 6. Gene expression after injury

Gene expression of inflammation, bone formation, bone resorption, and vascularization markers after injury and hindlimb unloading. All data from injured limbs are normalized by data from uninjured limbs to yield fold differences. The scale bar on the right indicates colors encoding fold changes relative to uninjured limbs: mean values lower than uninjured values are indicated in red, mean values greater than uninjured values are indicated in green. Black borders indicate significant differences from uninjured limbs ($p < 0.05$). Femur fracture resulted in upregulation of IL-6, BMP-2, OC, Runx-2, OPG, MMP-13, and VEGF by 7 days post-injury, while ACL rupture resulted in upregulation of OC and VEGF. HLU altered expression of several genes, notably IL-6, which was increased in HLU mice 3 days following femur fracture ($p = 0.005$), but decreased in HLU mice following ACL rupture (though not statistically significant). Listed p-values indicate a significant main effect of ambulation type (ground control (GC) or hindlimb unloading (HLU)) or a significant interaction between ambulation type and time point.